Photonic nanojet-enabled optical data storage

Soon-Cheol Kong,[1,*] Alan Sahakian,[1,2] Allen Taflove,[1] and Vadim Backman[2]

[1] *Department of Electrical Engineering and Computer Science, Northwestern University, Evanston, IL 60208, USA*
[2] *Department of Biomedical Engineering, Northwestern University, Evanston, IL 60208, USA*
[*] *Corresponding author: sch.kong@gmail.com*

Abstract: We show that our recently reported microwave photonic jet technique for detection of deeply subwavelength pits in a metal substrate can be extended to optical wavelengths for purposes of high-density data storage. Three-dimensional finite-difference time-domain computational solutions of Maxwell's equations are used to optimize the photonic nanojet and pit configuration to account for the Drude dispersion of an aluminum substrate in the spectral range near $\lambda = 400$ nm. Our results show that nanojet-illuminated pits having lateral dimensions of only $50\ \text{nm} \times 80\ \text{nm}$ yield a contrast ratio 27 dB greater than previously reported using a lens system for pits of similar area. Such pits are much smaller than BluRay™ features. The high detection contrast afforded by the photonic nanojet could potentially yield significant increases in data density and throughput relative to current commercial optical data-storage systems while retaining the basic geometry of the storage medium.

OCIS codes: (210.0210) Optical data storage; (230.3990) Micro-optical devices; (290.1350) Backscattering.

References and links

1. T. R. M. Sales, "Smallest focal spot," Phys. Rev. Lett. **81**, 3844-3847 (1998).
2. C. J. R. Sheppard, "Fundamentals of superresolution," Micron **38**, 165-169 (2007).
3. B. D. Terris, H. J. Mamin, D. Rugar, W. R. Studenmund, and G. S. Kino, "Near-field optical data storage using a solid immersion lens," Appl. Phys. Lett. **65**, 388-390 (1994).
4. C. A. Verschuren, D. M. Bruls, B. Yin, J. M. A. van den Eerenbeemd, and F. Zijp, "High-density near-field recording on cover-layer protected discs using an actuated 1.45 numerical aperture solid immersion lens in a robust and practical system," Japanese J. Appl. Phys **46**, 3889-3893 (2007).
5. R. Schmidt, C. A. Wurm, S. Jakobs, J. Engelhardt, A. Egner, and S. W. Hell, "Spherical nanosized focal spot unravels the interior of cells," Nature Methods **5**, 539-544 (2008).
6. Z. Chen, A. Taflove, and V. Backman, "Photonic nanojet enhancement of backscattering of light by nanoparticles: A potential novel visible-light ultramicroscopy technique," Opt. Express **12**, 1214-1220 (2004).
7. X. Li, Z. Chen, A. Taflove, and V. Backman, "Optical analysis of nanoparticles via enhanced backscattering facilitated by 3-D photonic nanojets," Opt. Express **13**, 526-533 (2005).
8. S. Lecler, Y. Takakura, and P. Meyrueis, "Properties of a three-dimensional photonic jet," Opt. Lett. **30**, 2641-2643 (2005).
9. A. V. Itagi and W. A. Challener, "Optics of photonic nanojets," J. Opt. Soc. Am. A **22**, 2847-2858 (2005).
10. Z. G. Chen, X. Li, A. Taflove, and V. Backman, "Superenhanced backscattering of light by nanoparticles," *Optics Lett.* **31**(2): 196-198, Jan. 15, 2006.
11. A. Heifetz, K. Huang, A. V. Sahakian, X. Li, A. Taflove, and V. Backman, "Experimental confirmation of backscattering enhancement induced by a photonic jet," Appl. Phys. Lett. **89**, 221118 (2006).
12. A. M. Kapitonov and V. N. Astratov, "Observation of nanojet-induced modes with small propagation losses in chains of coupled spherical cavities," Opt. Lett. **32**, 409-411 (2007).
13. S. Lecler, S. Haacke, N. Lecong, O. Crégut, J.-L. Rehspringer, and C. Hirlimann, "Photonic jet driven non-linear optics: example of two-photon fluorescence enhancement by dielectric microspheres," Opt. Express **15**, 4935-4942 (2007).

#96885 - $15.00 USD Received 5 Jun 2008; revised 12 Jul 2008; accepted 16 Jul 2008; published 21 Aug 2008

14. W. Wu, A. Katsnelson, O. G. Memis, and H. Mohseni, "A deep sub-wavelength process for the formation of highly uniform arrays of nanoholes and nanopillars," Nanotechnology **18**, 485302 (2007).
15. A. Heifetz, J. J. Simpson, S.-C. Kong, A. Taflove, and V. Backman, "Subdiffraction optical resolution of a gold nanosphere located within the nanojet of a Mie-resonant dielectric microsphere," Opt. Express **15**, 17334-17342 (2007).
16. M. Gerlach, Y. P. Rakovich, and J. F. Donegan, "Nanojets and directional emission in symmetric photonic molecules," Opt. Express **15**, 17343-17350 (2007).
17. P. Ferrand, J. Wenger, A. Devilez, M. Pianta, B. Stout, N. Bonod, E. Popov, and H. Rigneault, "Direct imaging of photonic nanojets," Opt. Express **16**, 6930-6940 (2008).
18. S.-C. Kong, A. V. Sahakian, A. Heifetz, A. Taflove, and V. Backman, "Robust detection of deeply subwavelength pits in simulated optical data-storage disks using photonic jets," Appl. Phys. Lett. **92**, 211102 (2008).
19. A. Taflove, and S. C. Hagness, *Computational Electrodynamics: The Finite-Difference Time-Domain Method*, 3rd ed. (Artech, Boston, MA 2005).
20. S.-C. Kong, J. J. Simpson, and V. Backman, "ADE-FDTD scattered-field formulation for dispersive materials," IEEE Microwave Wireless Comp. Lett. **18**, 4-6 (2008).
21. J. P. Berenger, "A perfectly matched layer for the absorption of electromagnetic waves," J. Comp. Phys. **114**, 185-200 (1994).
22. M. A. Ordal, L. L. Long, R. J. Bell, S. E. Bell, R. R. Bell, R. W. Alexander, Jr., and C. A. Ward, "Optical properties of the metals Al, Co, Cu, Au, Fe, Pb, Ni, Pd, Pt, Ag, Ti, and W in the infrared and far infrared," Appl. Opt. **22**, 1099 (1983).
23. J. A. C. Veerman, A. J. H. Wachters, A. M. van der Lee, and H. P. Urbach, "Rigorous 3D calculation of effects of pit structure in TwoDOS systems," Opt. Express **15**, 2075-2097 (2007).
24. Online: http://www.optotronics.com/b-lithium-ion.php
25. Online: http://statusreports.atp.nist.gov/reports/94-01-0115.htm

1. Introduction

Obtaining the finest possible optical resolution [1, 2], with specific potential applications to high-density optical data storage [3, 4] and microscopy [5], has been a long-time area of active research. In this paper, we propose new techniques for high-density optical data storage based upon the *photonic nanojet* [6–18]. The proposed techniques may permit significantly increased data density and throughput relative to current technology while retaining the basic geometry of the optical storage medium.

The photonic nanojet is an intense, narrow beam emerging from the back surface of a plane-wave-illuminated lossless dielectric cylinder or sphere of diameter greater than approximately 1 wavelength (λ). This beam appears for a wide range of diameters of the cylinder or sphere if the refractive index contrast relative to the surrounding medium is less than about 2:1. The nanojet propagates with little divergence for several λ into the surrounding medium while maintaining a transverse beamwidth smaller than λ. In fact, a transverse beamwidth as small as 0.3λ has been reported [15]. The present research was motivated by a key nanojet phenomenon, its *giant backscattering perturbation*. Namely, inserting a tiny ($\sim\lambda_e/_e100$ diameter) particle within the nanojet perturbs the backscattered power of the cylinder or sphere emitting the nanojet by an amount that is comparable to the *total* backscattered power of the cylinder or sphere [7, 10, 11].

In a recent paper [18], we reported the results of dimensionally scaled microwave laboratory experiments at 30 GHz which investigated the potential use of the photonic jet to detect deeply subwavelength pits in an optical data-storage disk. Pits and lands of appropriately scaled dimensions relative to the 1-cm wavelength were machined in an aluminum plate coated with a low-loss dielectric having an optimized thickness. To support the experiments, three-dimensional (3-D) finite-difference time-domain (FDTD) Maxwell's equations computational models [19] were also implemented. Our measurements and FDTD models both showed that pits having a very-small lateral area of $\lambda^2/40$ can be robustly detected with a contrast ratio approaching 30 dB relative to the no-pit case.

#96885 - $15.00 USD Received 5 Jun 2008; revised 12 Jul 2008; accepted 16 Jul 2008; published 21 Aug 2008

In this paper, we extend these microwave results to optical wavelengths. We again implement 3-D FDTD computational solutions of Maxwell's equations, but now optimize the photonic nanojet and pit configuration to account for the Drude dispersion of the aluminum substrate in a spectral range near $\lambda = 400$ nm. To model the Drude dispersion, we employ the auxiliary differential equation scheme for the pure scattered-field formulation of FDTD presented in [20], along with a standard perfectly matched layer absorbing outer grid boundary condition [21]. We assume values for the Drude plasma angular frequency ω_p and collision frequency γ_p reported in [22].

Our new 3-D FDTD Maxwell's equations computational models indicate that the effects of the Drude dispersion of the aluminum layer near $\lambda = 400$ nm can be compensated to yield a robust detection of deeply subwavelength pits comparable to what we measured in our previous microwave experiments. In fact, we have determined that nanojet-illuminated pits having lateral dimensions of only $50\ \text{nm} \times 80\ \text{nm}$ yield a contrast ratio fully 27 dB greater than previously reported using a lens system for pits of similar area [23]. (Such pits are much smaller than BluRay™ features.) This high contrast is a consequence of the nanojet's giant backscattering perturbation phenomenon.

Furthermore, as indicated by our FDTD modeling, the high contrast afforded by the photonic nanojet facilitates accessing multiple data values (potentially 10 or more) within a single nanojet footprint using either pit-depth coding or pit-pair separation coding. This could potentially yield significant increases in data density and throughput relative to current commercial systems while retaining the basic geometry of the optical storage medium.

2. Modeled geometry

Figure 1 illustrates (not to scale) the cross-section and dimensions of our proposed scheme for reading optical data using the photonic nanojet.

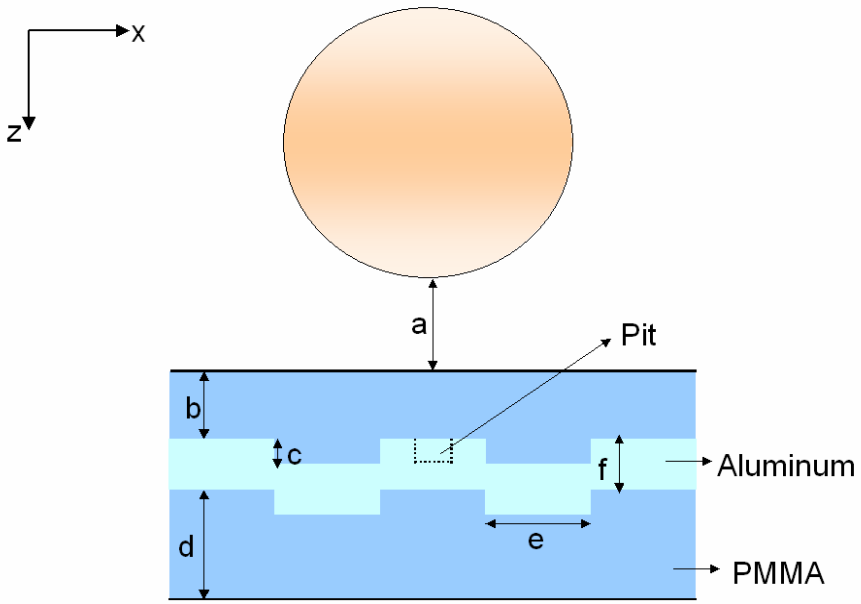

Fig. 1. Cross-section (not to scale) of the proposed optical data-storage geometry. The microsphere diameter is 2 μm. a = 160 nm, b = 480 nm, c = 40 nm, d = 360 nm, e =160 nm, f = 200 nm.

#96885 - $15.00 USD Received 5 Jun 2008; revised 12 Jul 2008; accepted 16 Jul 2008; published 21 Aug 2008

In Fig. 1, a 2-μm diameter polystyrene microsphere of refractive index n = 1.59 is placed 160 nm (a) above the optical data-storage medium. This medium is comprised of a grooved 200-nm thick aluminum layer (f) embedded within polymethyl methacrylate– PMMA (b = 480 nm, d = 360 nm). The groove periodicity is 320 nm (2e), and the groove height is 40 nm (c). 10.5 groove periods are modeled. The dotted line in the groove designates a pit, which is assumed to be filled with PMMA. Aluminum layer thickness is maintained in the presence of each pit. Illumination is assumed to be an x-polarized plane wave propagating in the +z-direction.

The entire FDTD computational modeling space spans $4\,\mu\text{m} \times 4\,\mu\text{m} \times 4\,\mu\text{m}$ with a uniform cubic grid-cell size of 10 nm. Our numerical convergence studies indicated that, using the FDTD Drude dispersion modeling technique presented in [20], a 10-nm grid-cell size provides an error of only ~0.1% in calculating the magnitude of the electromagnetic wave reflection coefficient of aluminum at λ = 400 nm. This is despite the skin depth of aluminum at this wavelength being comparable to the grid-cell size.

3. Computational results, optimizing the single-pit case

Figure 2 visualizes the FDTD-computed optical intensity (power density) normalized relative to the incident illumination for the isolated 2-μm diameter polystyrene microsphere illuminated at λ = 393.9 nm.

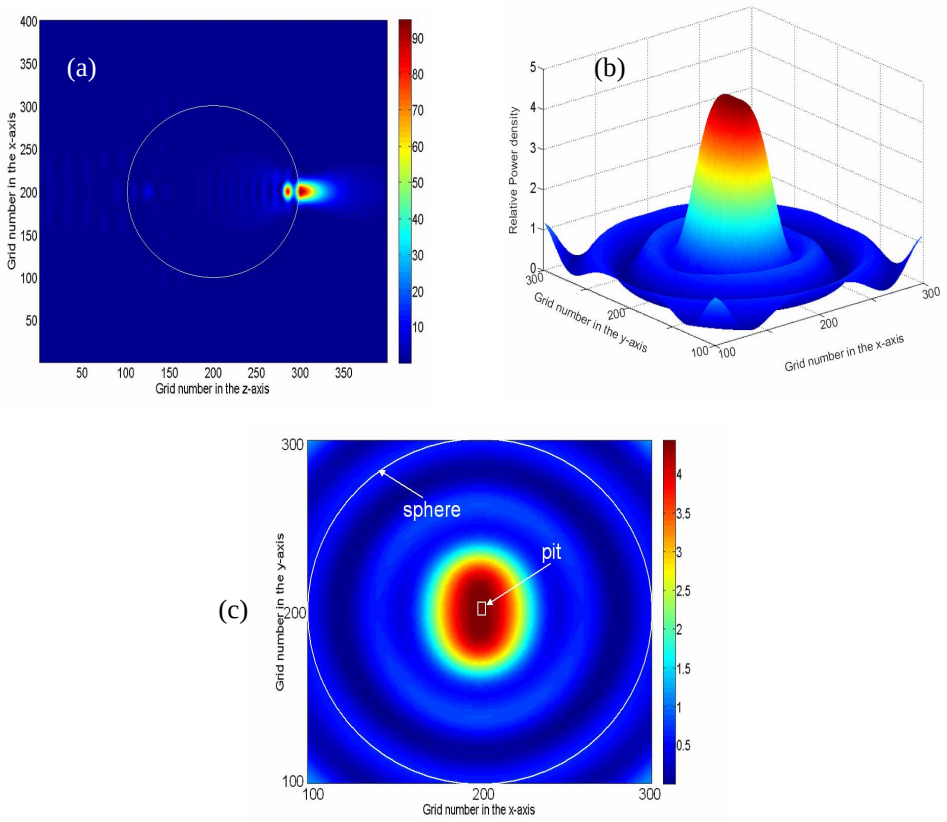

Fig. 2. FDTD-computed normalized optical intensity (power density) relative to the incident illumination for the isolated 2-μm diameter microsphere at λ = 393.9 nm. The cubic grid-cell size is 10 nm. (a) Photonic nanojet observed in the x-z longitudinal cut-plane. (b) 3-D plot in the x-y transverse plane located 600 nm from the back surface of the microsphere. (c) 2-D plot corresponding to (b).

#96885 - $15.00 USD Received 5 Jun 2008; revised 12 Jul 2008; accepted 16 Jul 2008; published 21 Aug 2008

Figure 2(a) depicts the photonic nanojet in the *x*-*z* longitudinal cut plane. Figure 2(b) is a 3-D surface plot of the normalized nanojet intensity in the *x*-*y* transverse cut-plane located 600 nm from the back-side surface of the microsphere (approximately at the same distance from the microsphere that the data-storage pit is located in subsequent FDTD models). Figure 2(c) is a 2-D plot corresponding to Fig. 2(b) which juxtaposes the nanojet's elliptical power-density distribution with: (1) the circular microsphere perimeter; and (2) a single rectangular data-storage pit incorporated in the subsequent fully populated FDTD models. From this figure, we see that the nanojet excites the data pit with a peak intensity of approximately four-times that of the incident plane wave.

We next consider the nanojet illumination of a single rectangular 50 nm × 80 nm (lateral cross-section) pit in the complete optical data-storage model of Fig. 1. Figure 3 graphs as a function of the nanojet wavelength and the pit depth the ratio of the FDTD-computed backscattered far-field power with no pit present to the computed backscattered far-field power with a single pit present.

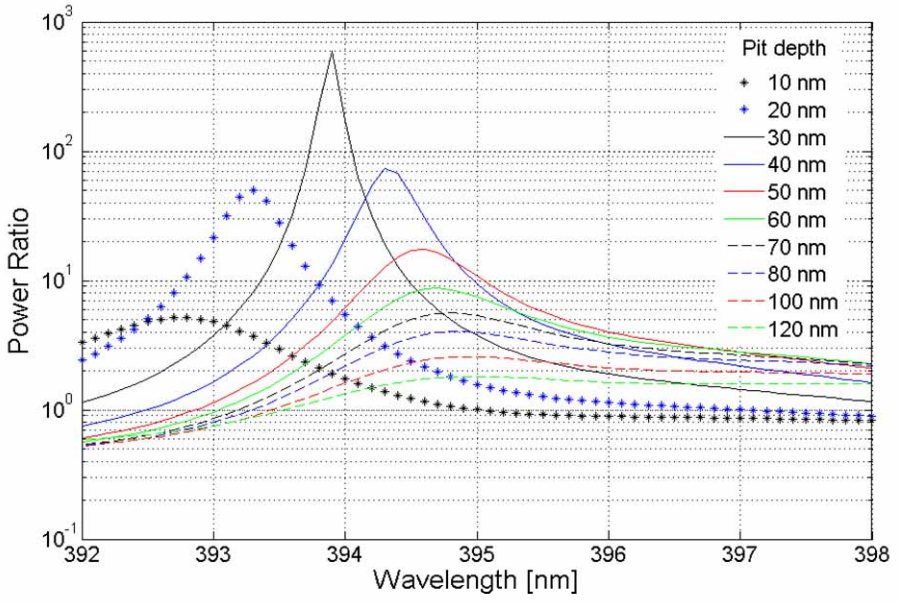

Fig. 3. FDTD-computed far-field no-pit / pit power ratio as a function of the nanojet wavelength and the pit depth for a single rectangular 50 nm × 80 nm (lateral cross-section) pit in the complete optical data-storage model of Fig. 1.

Figure 3 shows that the far-field no-pit / pit power ratio is generally greater than one, reaching a maximum value of ~600:1 (~28 dB) at λ = 393.9 nm for the optimum pit depth of 30 nm. This is approximately 500-times (27 dB) greater than the value reported in [23] using a lens system for an octagonal pit having a slightly larger lateral area in square wavelengths. We note that the curves in Fig. 3 are essentially unchanged if a separation of 420 nm or more is maintained between adjacent pits. This is the near zero-crosstalk criterion.

From Fig. 3, we see that the no-pit / pit power-ratio characteristic for the optimum pit depth is sharply peaked at λ = 393.9 nm. It is clear that taking full advantage of the high peak value of this power-ratio characteristic requires a laser spectral linewidth that is sufficiently less than the width of this characteristic. An example of a commercially available blue (λ = 473 nm) continuous-wave laser diode having an appropriate spectral linewidth (< 0.1 nm) for this purpose is found in [24], a laser pointer powered by a 3.7 volt lithium-ion battery.

#96885 - $15.00 USD Received 5 Jun 2008; revised 12 Jul 2008; accepted 16 Jul 2008; published 21 Aug 2008

4. Increased data-storage density via pit-depth coding

For a fixed nanojet wavelength $\lambda = 393.9$ nm, Fig. 4 graphs as a function of pit depth (for pit depths greater than 30 nm) the FDTD-computed far-field no-pit / pit power-ratio characteristic for the 50 nm × 80 nm pit studied in Fig. 3. The observed monotonic decrease in this power ratio over a wide dynamic range suggests the possibility of a pit-depth coding scheme [25] wherein multiple data levels are encoded at the location of a single pit according to its depth, thereby increasing the overall data-storage capacity and retrieval speed.

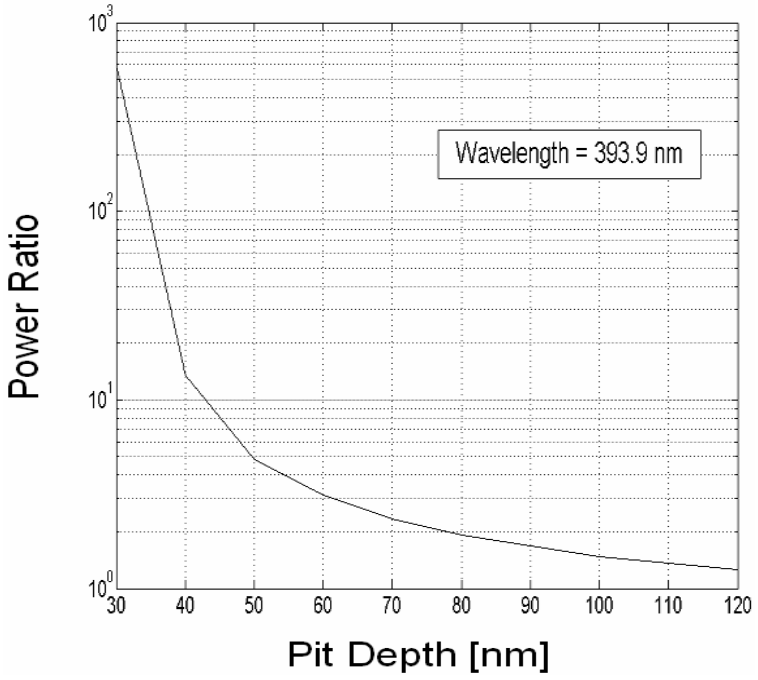

Fig. 4. FDTD-computed far-field no-pit / pit power ratio vs. pit depth for a 50 nm × 80 nm lateral cross-section pit at the fixed wavelength $\lambda = 393.9$ nm. The monotonic nature of this characteristic over a wide range of power ratios and ~90 nm of pit-depth variation suggests a pit-depth coding scheme wherein multiple data levels are encoded at the location of a single pit according to its depth.

5. Increased data-storage density via pit-pair separation coding

We last consider a pair of 50 nm × 80 nm rectangular pits, each having the optimum pit depth of 30 nm. The two pits are assumed to be positioned lengthwise along the *y*-direction centered within the nanojet's footprint shown in Fig. 2(c). A variable pit-to-pit separation is analyzed using FDTD modeling.

For a fixed nanojet wavelength $\lambda = 393.9$ nm, Fig. 5 graphs the FDTD-computed far-field no-pits / pits power-ratio as a function of the pit-to-pit separation. The observed monotonic increase in this power ratio over a wide dynamic range suggests the possibility of a pit-pair separation coding scheme wherein multiple data levels are encoded within a single nanojet footprint according to the separation of the pair of pits within that footprint.

Pit-pair separation coding may permit more encoded data levels than pit-depth coding. While both schemes quantize over the same wide range of backscattered power, the pit-pair separation coding scheme quantizes over a distance metric of ~300 nm, which is about three-times the ~90 nm depth metric quantized by the pit-depth coding scheme.

#96885 - $15.00 USD Received 5 Jun 2008; revised 12 Jul 2008; accepted 16 Jul 2008; published 21 Aug 2008

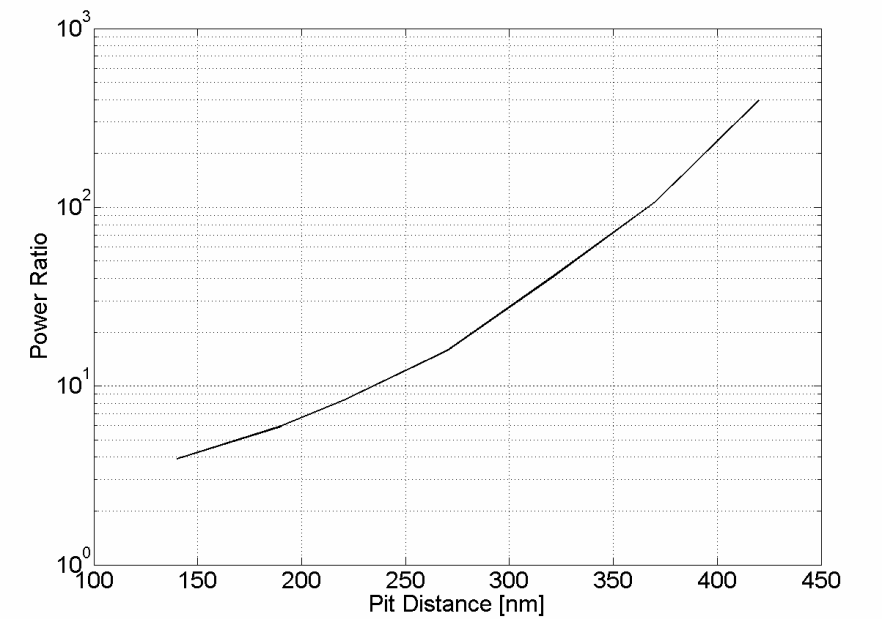

Fig. 5. FDTD-computed far-field no-pits / pits power ratio vs. pit-to-pit separation for a pair of $50\text{ nm} \times 80\text{ nm}$ rectangular pits, each having the optimum pit depth of 30 nm. The wavelength is fixed at $\lambda = 393.9$ nm. The two pits are assumed to be positioned lengthwise along the *y*-direction centered within the nanojet's footprint shown in Fig. 2(c). The monotonic nature of this characteristic over a wide range of power ratios and ~300 nm of pit-to-pit separation suggests a scheme wherein multiple data levels are encoded at the location of a single pit-pair within the nanojet footprint according to the pit-to-pit separation distance.

6. Summary, discussion, and ongoing work

We have shown that our recently reported microwave photonic jet technique for detecting deeply subwavelength pits in a metal substrate can be extended to optical wavelengths for purposes of high-density data storage. We implemented 3-D FDTD computational solutions of Maxwell's equations to optimize the photonic nanojet and pit configuration to account for the Drude dispersion of an aluminum substrate in the spectral range near $\lambda = 400$ nm. Our computational models indicate that substrate pits having a lateral area of 0.025 square wavelengths, i.e., much smaller than current BluRay™ device features, can be robustly detected with a contrast ratio approximately 27 dB greater than that provided by a lens system. The large monotonic no-pit / pit power ratios achieved using the nanojet suggest the possibility of encoding multiple data levels within the nanojet footprint using either pit-depth coding or pit-pair separation coding.

In ongoing work, we are conducting finer-resolution FDTD simulations to examine the sensitivity of our proposed nanojet-enabled optical data-storage technique to fluctuations of the head-to-media spacing (reported to be < 3 nm, even at 3000 rpm [4]). In this regard, we are also studying the use of a silica microsphere that generates a longer nanojet which would allow increasing the head-to-media spacing. Finally, we are using FDTD modeling to study sensitivities to reported state-of-the-art levels of radial and azimuthal tilts of the media.

Acknowledgments

This work was supported in part by NSF Grants CBET-0522639 and CBET-0733868. Jim Spadaro and Nikola Borisov managed and maintained Prof. Backman's computer cluster.

#96885 - $15.00 USD Received 5 Jun 2008; revised 12 Jul 2008; accepted 16 Jul 2008; published 21 Aug 2008